



Friction and wear optimization of SiC/graphite reinforced AZ31 hybrid composite using Taguchi method

Itha Veeranjanyulu¹ · V. Haripriya² · Rajasekaran Saminathan³ · B. Vishnu Vardhana Naidu⁴ · J. Justin Maria Hillary⁵ · Adina Srinivasa Vara Prasad⁶ · P. Satishkumar⁷ · B. Ch. Nookaraju⁸ · Ram Subbiah⁸

Received: 22 August 2023 / Accepted: 24 November 2023 / Published online: 22 December 2023
© The Author(s), under exclusive licence to Springer-Verlag France SAS, part of Springer Nature 2023

Abstract

In this work, hybrid nanocomposites were successfully fabricated using a stir casting machine setup with a weight of 3%, 5%, and 7%. Additionally, 7% hybrid nanocomposite was tested for wear behavior under the wear test setup. The experimental parameters were 15–35 N load, 136–409 rpm speed, and 150–450 m distance. Based on controlling variables, including load, speed, and distance, ANOVA was used to analyze how the most significant variables affected the wear rate (WR) and coefficient of friction (COF). The outcomes were assessed using MINITAB Software. S/N Ratio analysis was used to establish the best parameter combination to lower the WR and COF. The WR of specimen was increases as the sliding distance rises. The wear rate of the composites exhibits an increase with higher normal loads. Due to the high interaction between the surfaces of matrix alloy (AZ31) and reinforcements (SiC, Gr), the metallurgical properties of the seven wt% SiC/Gr alloy performed better than those of the base alloy. The microstructure of the worn surface was examined by SEM, and the particles were described by EDS. The maximum amount of wear rate (320 μm) was observed at a maximum load of 35N, speed 409 rpm with sliding distance of 300 m, while the minimum amount of wear rate (79 μm) was found at a minimum load of 15N, speed 136 rpm with sliding distance of 150 m.

Keywords Hybrid nanocomposite · Pin on disc tribometer · Wear rate · COF · ANOVA and Taguchi method

✉ P. Satishkumar
sp.sathishkumar10@gmail.com

Itha Veeranjanyulu
anjimech@gmail.com

V. Haripriya
drharipriyavadapalli@gmail.com

Rajasekaran Saminathan
rsaminathan@jazanu.edu.sa

B. Vishnu Vardhana Naidu
vishnu234@gmail.com

J. Justin Maria Hillary
justinhillarymech@gmail.com

Adina Srinivasa Vara Prasad
adina.srinivas301@gmail.com

B. Ch. Nookaraju
nookaraju@griet.ac.in

¹ Department of Mechanical Engineering, Aditya Engineering College, Surampalem, India

² Department of Humanities and Sciences, MLR Institute of Technology, Dundigal, Hyderabad 500043, Telangana, India

1 Introduction

Nanocomposites have recently been in high demand in the various fields of applications, because of their superior qualities, including their excellent strength, lightness, stiffness,

³ Department of Mechanical Engineering, College of Engineering, Jazan University, Jazan, Saudi Arabia

⁴ Department of Mechanical Engineering, Sree Vidyanikethan Engineering College, Mohan Babu University, Sree Sainath Nagar, A. Rangampet, Tirupati, Andhra Pradesh 517102, India

⁵ Department of Mechatronics Engineering, Sri Krishna College of Engineering and Technology, Coimbatore, India

⁶ Department of Mechanical Engineering, Shri Vishnu Engineering College for Women, Bhimavaram, Andhra Pradesh, India

⁷ Department of Mechanical Engineering, Rathinam Technical Campus, Coimbatore, Tamilnadu, India

⁸ Department of Mechanical Engineering, Gokaraju Rangaraju Institute of Engineering and Technology, Hyderabad, India

and improved thermal characteristics [1, 2]. The magnesium properties, such as wear and fatigue resistance, were enhanced by adding reinforced particles. Magnesium and its alloys have high rigidity and strength, a critical property in various applications. Ceramic particles improved the mechanical properties compared to other reinforcements [3, 4]. A new material for diverse engineering structural applications is the AZ31 alloy, one of the several alloys in the AZ family. It is because of its distinctive qualities, including more strength and stiffness. However, AZ series alloys have attained significantly less wear resistance and COF. Hence, to enhance these properties, alloys were made with reinforcement particles such as SiC [5, 6], Graphite [7], Al₂O₃ B₄C-WC-ZrO₂ [8], and Ti [9] at micro and nano size. SiC and Gr have provided good wettability and solid lubricant in magnesium to enhance the wear resistance. Hence, the AZ31D matrix was incorporated with SiC and graphite nanoparticles to improve the tribological properties. Magnesium-based nanocomposites are becoming more common in recent years due to their increased wear resistance. Friction stir processing [10], Combined Stir and squeeze casting [11, 12], Hot extrusion process [11], powder metallurgy [13], mechanical alloying [14], thermo mechanical processing [15] are commonly employed to develop the MMCs. Due to its advantages, such as simplicity and adaptability, the stir casting technique is preferred; mass production can be done more affordably.

Using Taguchi grey relational analysis, Srinivasan et al. [16] adjusted the control inputs on WR and COF of composites. They discovered that the adequate parameter inputs for obtaining the minimal WR and COF is 12 wt% AlN. Swamy et al. [17] studied the eutectic composites using a wear test setup and found that the WR and friction coefficients lowered with time as the wt. % of graphite parts increased. These results established the graphite film, which works as a lubricant in the composite. Balaji et al. [18] used Taguchi with RSM to optimize the nano grain-refined composites and reported that the load was the most prominent parameter for analyzing the specific WR. The impact of SiCnp on the matrix was studied by Subramani et al. [19], and they noticed that the SiCnp enhanced the hardness and WR. In the investigation of wear resistance, Sandeep Kumar et al. [20] noticed that the load was the critical parameter to determining the WR and looked at the worn-out surface of manufactured hybrid composites.

Gnanavelbabu et al. [21] discussed the effects of ultrasonic power on nanocomposites and found that the composite manufactured at 2500 W had a lower WR and COF than other composites under all sliding situations. Ambigai et al. [22] improved the WR and COF of the LM6 hybrid nanocomposite in dry sliding conditions. When compared to nanocomposite, they found that the WR and COF for hybrid composite reduced by 25% and 15%, respectively,

and that abrasive wear mechanisms were more common for hybrid composite than for nanocomposite. Stir-cast hybrid composites were created, and their two-body abrasive wear behavior was examined by Kaushik et al. [23]. They concluded that the WR of the hybrid composite was enhanced with an addition of Gr. Using a liquid state technique, Suresh et al. [24] studied the WR of nanocomposite and discovered that when the SiCnp increases from 1 to 4 wt%, the WR reduces linearly. For worn-out samples, SEM was used. Xiao et al. [25] explored the impact of titanium diboride reinforcement on the WR of composite in different situations and concluded that the composite has better WR. Using Taguchi method, the effect of wear properties in composites reinforced with AZ31B and ZrSiO₄ were investigated. Dry sliding wear experiments were conducted using an L9 orthogonal array (OA) design on a pin-on-disk apparatus. Microstructural analysis indicated the presence of ZrSiO₄ particles, which had a mitigating effect on wear in the specimens. The ANOVA study identified wear rate as a significant parameter affecting the composite properties [26]. This study examined the COF and wear properties of polyester composites. In this work, various control parameters were used to investigate the wear analysis [27]. According to Mohammed et al. [28], the load has more impacted on WR as compared to other parameters. Kumar et al. [29] explored that lower WR was obtained in hybrid composites than in composite materials due to lower material dispossession and the addition of graphite powder into composites. Kumar et al. [30] investigated the MMC using Taguchi design and concluded that an abrasive wear mechanism plays the most prominent role on the surface of a specimen.

The Taguchi analysis was designed with three control variables—the load, speed, and distance—is currently being investigated to enhance the wear behavior of hybrid nanocomposite materials. These input parameters were selected based on the analysis of previous works [28, 29]. ANOVA has been used to evaluate the impact of influential factors on WR and COF. Hybrid composites (AZ31-SiC-Gr) are utilized in frictional applications including clutches and brakes. These have excellent wear resistance, high strength, and low mass, which make them potential for usage in automotive applications.

The key novelty in this research lies in its investigation of the both effect of SiC and Gr nanoparticles on the wear characteristics of AZ31 magnesium alloys. Prior studies primarily concentrated on single nanoparticle additives, whereas this research explores the simultaneous integration of SiC and graphite, harnessing their complementary properties. SiC bolsters hardness and wear resistance, while graphite provides solid lubrication. This dual reinforcement strategy is expected to produce a unique composite material with synergistic wear-resistant characteristics. The stir casting method,

used for uniform dispersion of nanoparticles, ensures effective synergy between the two additives. Consequently, this work presents a fresh, innovative solution for enhancing wear resistance in AZ31 alloys, offering promising applications across various industries. The majority of research has focused on aluminum and magnesium alloy matrix with various reinforcements, such as B_4C , Al_2O_3 , SiC, WC, TiC, and Gr, according to the thorough works of literature, but none of them has attempted to use AZ31 with nano-sized SiC/Gr as reinforcement composites. Therefore, the aim is to minimize the WR and COF of a stir-cast nanoSiC/Gr-filled AZ31 matrix composite with the best possible parameters. Minitab software is a data analysis tool designed for comprehending data and making better decisions. It performs numerous statistical tests such as regression analysis, ANOVA, and t-tests. To clearly depict data, graphs, and charts may also be made with Minitab.

2 Experimental setup

2.1 Materials and methods

AZ31 matrix reinforced with SiC and Gr with average particle size of 53 nm, and 75 nm respectively. The matrix alloy was purchased in ingot form; SiC and graphite were brought in nanopowder form. The elements of AZ31 matrix alloy were shown in Table 1.

In order to create hybrid nanocomposites, stir casting was used. The furnace temperature was increased around 650 °C before the ingredients were packed in the crucible, which has been preheated to 400 °C. The standard stirrer rotated at a speed of 700 rpm. The argon gas is supplied continuously to prevent chemical reactions in the process of materials getting into liquid state. The molten composite was poured in to die. At room temperature, the nanocomposites were quenched. The stress was eliminated through homogenization in 24 h.

A disc polishing machine and various grades of polishing paper were used to prepare the manufactured sample. Etchant was subsequently employed to eliminate contaminants from the top of the specimen. The SEM image and micrograph of the nanocomposite was studied by using SEM. The elemental breakdown of the alloy and nanocomposite was determined by EDS analysis. All samples' microhardness was measured using a Vickers microhardness tester. UTM (INSTRON-E1025) was used to measure specimens' tensile and compressive properties.

The experiment was performed on a wear test setup (TR-201) under dry sliding conditions, and line diagrams were shown in Fig. 1 and Fig. 2, respectively. The specifications of the wear test are as follows:

Manufacturer: Ducom Ltd., Chennai; Load range: up to 120 N; Disc Speed: 100–2000 rpm; Wear track diameter:

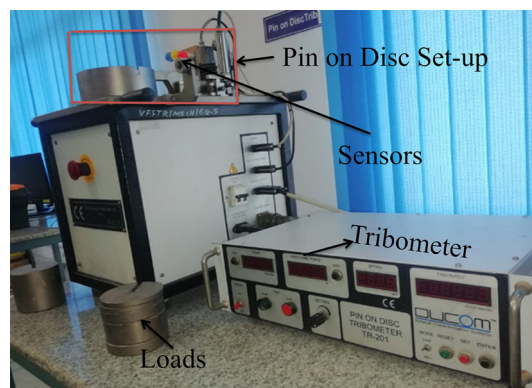


Fig. 1 Wear test (Pin on disc tribometer) set-up

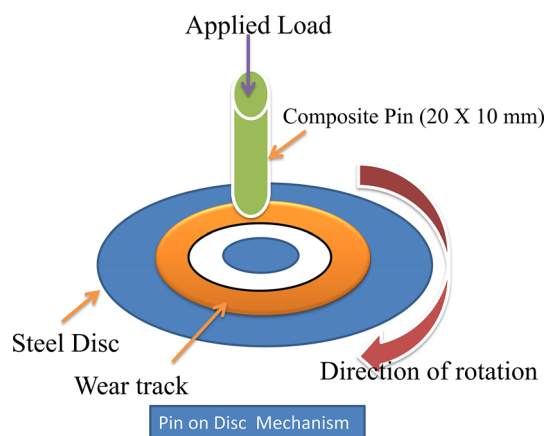


Fig. 2 Line diagram of Wear test

10–120 mm; Specimen pin diameter: 10–12 mm; Pin length: 25–30 mm.

The specimen is placed in a pin holder and kept at the right angle to the disk (made of EN31 steel of hardness 62 HRC), providing sliding action [23]. The size of the sample is 10 mm diameter, and 25 mm length is placed against EN31 steel disc, according to ASTM G99 standard. It is important to remember that the test sample's end surfaces were polished before testing. The experiment was performed at different levels with the same track diameter of 70 mm, and several input variables, including load, speed, and distance, were changed within the range shown in Table 2. By observing the movement of the arm, a linear variable differential transformer assists in determining the output results of wear rate (μm) and frictional force (N). Each specimen's weight loss was measured using an electronic digital scale. At every experiment, the steel disc was completely cleaned with a solution of an acetone before. The weight loss determined WR, and COF was calculated using Eq. (1). The surface morphologies of the pins are studied using SEM after the wear test.

$$(\text{COF}) = \frac{\text{Frictional force in N}}{\text{Normal force in N}} \quad (1)$$

Table 1 Elements of AZ31 in wt%

Elements	Al	Zn	Mn	Cu	Fe	Ni	Si	Mg
Wt%	3	0.98	0.2	0.002	0.002	< 0.001	< 0.01	Rest

Table 2 Experimental results and S/N ratios

Experiment	Load (N)	Speed (rpm)	Distance (m)	Wear rate (μm)		COF	
				Measured Value	S/N ratio	Measured Value	S/N ratio
1	15	136	150	79	-41.2892	0.15	16.47817
2	15	273	300	116	-37.9525	0.12	18.41638
3	15	409	450	92	-39.2758	0.31	10.17277
4	25	136	300	131	-42.3454	0.27	11.37272
5	25	273	450	188	-45.4832	0.29	10.75204
6	25	409	150	235	-47.4214	0.3	10.45757
7	35	136	450	142	-43.0458	0.31	10.17277
8	35	273	150	237	-50.103	0.28	11.05684
9	35	409	300	320	-47.495	0.27	11.37272

2.2 Taguchi method

The experiment was conducted with taguchi L9 design based on three levels. It is a systematic approach for optimizing processes and products by identifying the most influential factors with a minimal number of experiments. It employs a nine-factor, three-level orthogonal array design to efficiently explore parameter variations and their effects on a specific output or response variable. By systematically varying factors at different levels, the L9 Taguchi method helps determine which combination yields the best or most robust results while minimizing the required trials. Industries widely use this method to improve quality and performance while reducing experimentation time and costs. In this method, DOE was depending upon the input factors. In this statistical investigation, Taguchi L9 (3^3) OA was selected. Taguchi calculated the S/N ratio for each experimental setting [30]. The higher S/N ratio is determines the level of process parameters that should be used. In the present investigation, the input parameters are load, speed (136 rpm, 273 rpm, and 409 rpm), and distance (150 m, 300 m, and 450 m) have been selected and set at three levels. Finally, the optimum parameter setting was designed by ANOVA with help of MINITAB software [31].

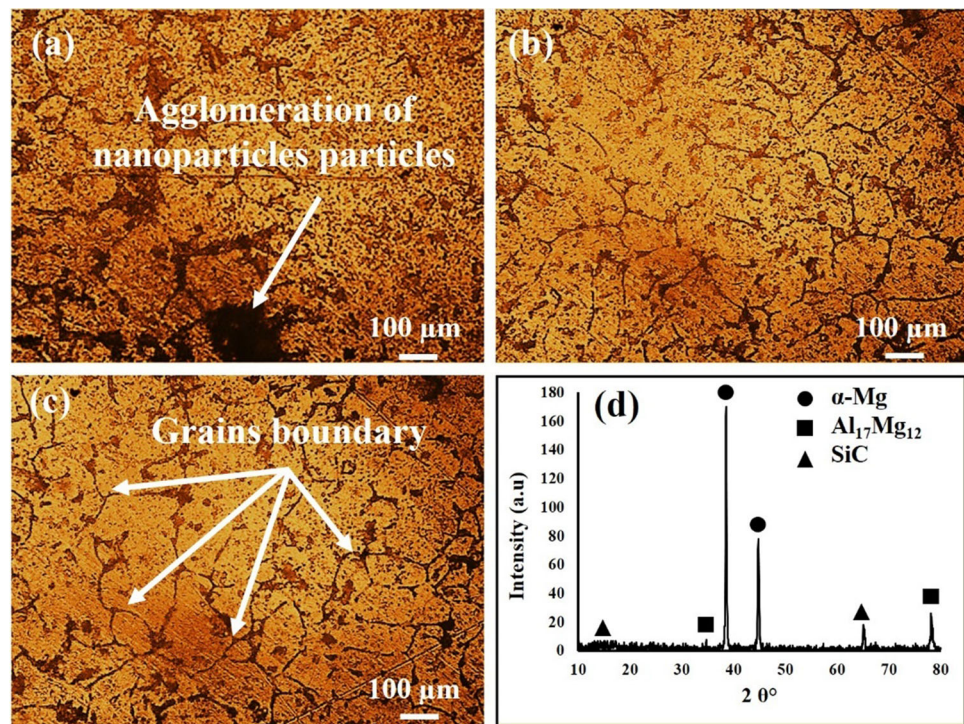
3 Results and discussions

According to the mechanical characterization findings, the base alloy's TS, CS, and hardness were all improved by 68%, 107%, and 54%, respectively, when it reaches an optimal proportion of 7% nanocomposite. The detailed investigation of

mechanical properties was carried out in the previous article [32]. Design of experiment (DOE) was conducted at three levels with nine experiments. S/N ratio plot, 3D surface plot, Contour plot and residual plot were drawn using MINITAB software, from these results estimate the most influencing parameters on WR and COF. The results of specimens and S/N ratios were shown in Table 2.

Table 2 illustrates the variation in the composites' friction coefficient (μ) and SiC nanoparticles under three distinct applied loads. The data indicates a noticeable decrease in the friction coefficient as the speed increased under similar load conditions. However, this reduction becomes less significant when the distance increases. This phenomenon can be allocated to the self-lubricating properties of SiC_{np}. During wear tests, as SiC nanoparticles were extracted from the matrix, they came into direct contact with the counter material, minimizing the contact area portion between the both materials and consequently lowering the friction coefficient [33]. Table 2 reveals a decreased friction coefficient with increasing applied load under the same SiC nanoparticle content. It can be attributed to the heightened plowing force and penetration within the samples at higher applied load conditions. It increases SiC pull-out from the matrix, enhancing the lubricant's efficiency. Based on the data distribution in Table 2, the Boltzmann model was applied to fit the curves depicting the relationship between the COF and sliding distance. The high R^2 values of nearly 91.5% indicate the suitability of the Boltzmann model in accurately describing the relationship between the friction coefficient and SiC nanoparticles content [34]. The maximum amount of WR (320 μm) was observed at a maximum load of 35N, speed 409 rpm with distance of 300 m, while the minimum amount

Fig. 3 Optical microstructure of AZ31 hybrid composite reinforced by SiC/Graphite, (a) 7%, (b) 5%, (c) 3%, (d) XRD peaks at 7% reinforcement



of WR (79 μm) was built at a load of 15N, speed 136 rpm with distance of 150 m.

3.1 Micro structural analysis

The Optical images of the nanocomposite was shown in Fig. 3a-d. It reveals that the reinforcements were uniformly distributed along with the matrix alloy. The micrograph of nanocomposite observed that the groups of particles were concentrated in one location during polishing and grain boundaries were identified. Incorporating SiC and graphite nanoparticles at varying concentrations of 3%, 5%, and 7% into the AZ31 magnesium alloy by stir casting intensely impacts its microstructure, leading to significant changes in its mechanical and wear properties. At the lowest concentration of 3%, the SiC and graphite nanoparticles are dispersed within the magnesium matrix, resulting in a refined grain structure due to the fasten effect of these elements on grain fringes. It leads to an improvement in the alloy's hardness, strength, and WR. At the intermediate concentration of 5%, the microstructure becomes even more refined, with a more uniform distribution of nanoparticles. It further increases the alloy's mechanical properties, making it suitable for higher strength and durability applications. However, at the highest concentration of 7%, the microstructure experiences a transition from a uniform dispersion of nanoparticles to clustering, which can lead to localized regions of high hardness and enhance the wear properties.

The reinforcements were influences the precipitation behavior of secondary phases within the AZ31 magnesium alloy. The nanoparticles serve as nucleation sites for the formation of intermetallic compounds and precipitates, which can alter the alloy's overall microstructure. At 3% concentration, the nanoparticles promote the formation of fine precipitates, contributing to the alloy's age-hardening response and improved mechanical properties. However, as the nanoparticle concentration increases to 5% and 7%, leading to excessive precipitation and potential embrittlement. The combination of SiC and graphite nanoparticles can introduce synergistic effects on the microstructure of the AZ31 alloy. SiC nanoparticles enhance the alloy's strength and wear resistance, while graphite nanoparticles provide solid lubrication properties, reducing friction and wear. This synergistic effect can be optimized at an intermediate concentration of 5%, where both nanoparticles are well-distributed and contribute positively to the alloy's performance. X-ray diffraction (XRD) analysis of AZ31 magnesium alloy reinforced with 7% reinforcement particles revealed in Fig. 3d provides crucial insights into this advanced composite material's phase composition. This comprehensive analysis delves deep into the interplay between the base AZ31 alloy, the SiC reinforcement, and the presence of Graphite, shedding light on their roles and contributions. The dominant phase in the AZ31 magnesium alloy, $\text{Al}_{17}\text{Mg}_{12}$, is a crucial starting point for the XRD analysis. This phase constitutes the primary crystalline structure of the base material and is characterized by its specific atomic arrangement and lattice parameters.

Table 3 Response table for WR

Level	Load L (N)	Speed S (rpm)	Distance D (m)
1	−39.51	−40.61	−46.27
2	−40.81	−41.85	−40.98
3	−46.88	−44.73	−39.94
Delta	7.38	4.12	6.33
Rank	1	3	2

Table 4 Response table for COF

Level	Load L (N)	Speed S (rpm)	Distance D (m)
1	15.02	12.67	12.66
2	10.86	13.41	13.72
3	10.87	10.67	10.37
Delta	4.16	2.74	3.35
Rank	1	3	2

XRD is exceptionally adept at detecting and quantifying this phase's presence, offering precise information regarding its orientation, crystallinity, and potential alterations induced by the incorporation of nanoparticles. The SiC phase is pivotal in enhancing the alloy's properties. XRD analysis distinctly highlights the SiC peaks within the diffraction pattern, signifying the presence of this hard ceramic phase. These peaks' position, intensity, and breadth provide essential information regarding the size, distribution, and preferred orientation of the SiC nanoparticles within the AZ31 matrix. A well-dispersed and oriented SiC phase can significantly contribute to the alloy's mechanical strength, stiffness, and wear resistance, making its characterization through XRD vital for optimizing composite performance. An equally critical aspect of XRD analysis is the potential detection of interfaces or interactions between Al17Mg12, and SiC, phases. These interfaces may manifest as new diffraction peaks or shifts in existing ones, highlighting any bonding or chemical interactions between the elements. Understanding these interactions is fundamental to predicting the alloy's mechanical behavior, as they can influence the composite's load transfer mechanisms and overall performance [42–45].

EDS analysis of AZ31 magnesium alloy with 3% and 7% SiC and Graphite reinforcement was revealed in Fig. 4(a, b), focusing on major alloying elements Mg, Si, Al, and Zn provides valuable insights into the alloy's composition and distribution of reinforcing particles. In AZ31, Mg is the primary constituent, and EDS precisely quantifies its content while revealing the presence and dispersion of Si, Al, and Zn. When reinforced with SiC and Graphite, EDS discerns changes in the elemental composition due to incorporating these reinforcing materials. This analysis allows for a quantitative assessment of the alloy's composition, confirming the desired reinforcement content and ensuring the alloy's suitability. It can assume that there was no audible reaction during casting between the materials.

3.2 Taguchi analysis

Tables 3 and 4 indicate that the S/N ratio of the response table is smaller the better for the WR and COF. The WR

was most significantly affected by the load (rank 1), followed by distance (rank 2) and speed (rank 3). Figure 5 and 6 represents the S/N ratio plot of WR and COF, respectively. These graphs showed that the highest values are the optimum process parameter setting. Finally, it was concluded that the load (15 N), speed (136 rpm), and distance (450 mm) had been the maximum mean of the S/N ratio; therefore, the predicted optimum process parameter setup for obtaining low WR using the taguchi method is L1-S1-D3. Similarly, the optimum process parameter setup for obtaining low COF is L1-S2-D2. The change in optimum setting is due to surface cracks in the nanocomposite; because of this, the speed has been enhanced to 273 rpm, and the distance has to 300 mm. This method is used to analyze the outcomes of experiments. It was conducted for a level of confidence at 95%. ANOVA investigated the order of influencing parameters on WR and COF [26, 27]. The results of WR are listed in Table 5, whereas COF is listed in Table 6. The number of levels minus one obtained the degree of freedom (DF), the total considering three factors at three levels, so that error got 2. The contribution percentage is declared that the load contributes more to WR and COF, with 66.73% and 47.41%, respectively. The speed and distance have been less contributing to WR and COF than load. This value is determined using the Eq. (2).

$$\text{Percentage of contribution} = \left(\frac{\text{Seq SS}}{\text{Total}} \times 100 \right) \quad (2)$$

In the same way, the high-affecting parameters were also recognized based on the P value and F value [46, 47]. Finally, it recognizes that the load was the outstanding parameter influencing WR and COF.

3.3 Impact of process variables on WR and COF

The surface and contour plots of WR and COF are shown in Figs. 7, 8, 9 and 10. The optimum process parameter for low wear rate and COF was L1-S1-D3 and L1-S2-D2, respectively. Therefore, the plots were drawn at this condition. The surface plots of WR and COF vs. parameters are shown in Figs. 7a and b. In contrast, the curved line in Fig. 8a and b

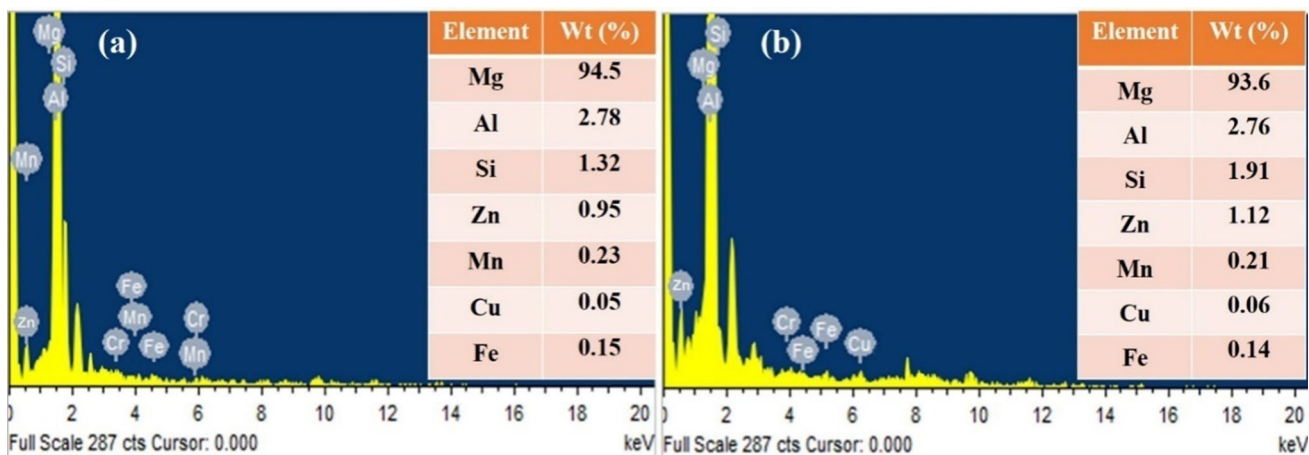
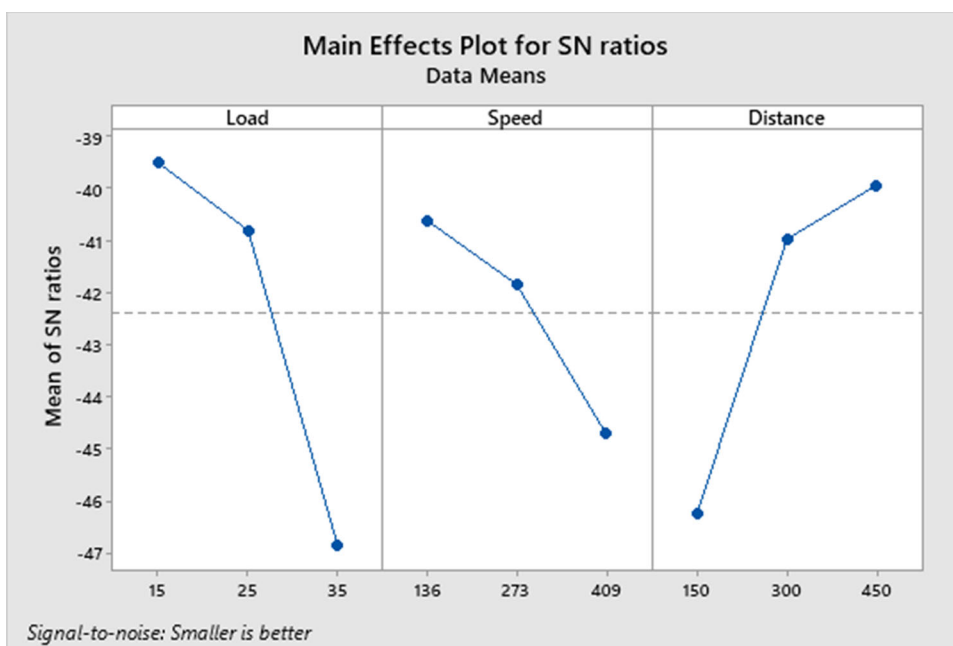


Fig. 4 EDS analysis of AZ31 hybrid composite reinforced by SiC/Graphite, (a) 3%, (b) 7%,

Fig. 5 Mean S/N ratio of wear rate



contour plots show the impact of the point where the SiC/Gr concentration meets the volumetric wear rate. The research’s surface and contour plots showed that the volumetric wear rate was minimal, at least under load [20, 22]. The presence of Gr particles that have been stripped from the composite and formed a thin coating at the edge of the opposite face, enhancing WR, is the main reason why the wear rate is reduced at a load of 15 N, speed of 136 rpm, and distance of 450 m. It can be seen that COF decreases as Parameters increase. The primary cause of COF falls may be due to the load increases, which causes the composites to soften, and as a result, COF has decreased due to lubricant. Here, the graphite serves as a lubricant [16].

3.4 Modeling

The linear regression analysis used Minitab to create the predictive equations in the current study. The dependent variables are WR and COF, which have a function of load, velocity, and distance, respectively. The linear regression equation was as shown in the Eq. (3) for WR and Eq. (4) for COF of hybrid composite, respectively. The developed models were checked by using the R^2 value. Usually, it varies from zero to 100%. If this value is close to 100%, it fits the variables well. The regression analysis concluded that R^2 for WR has better results than COF. Therefore, the evolved R^2 value for WR and COF was 91.49% and 56.04%, respec-

Fig. 6 Mean S/N ratio of COF

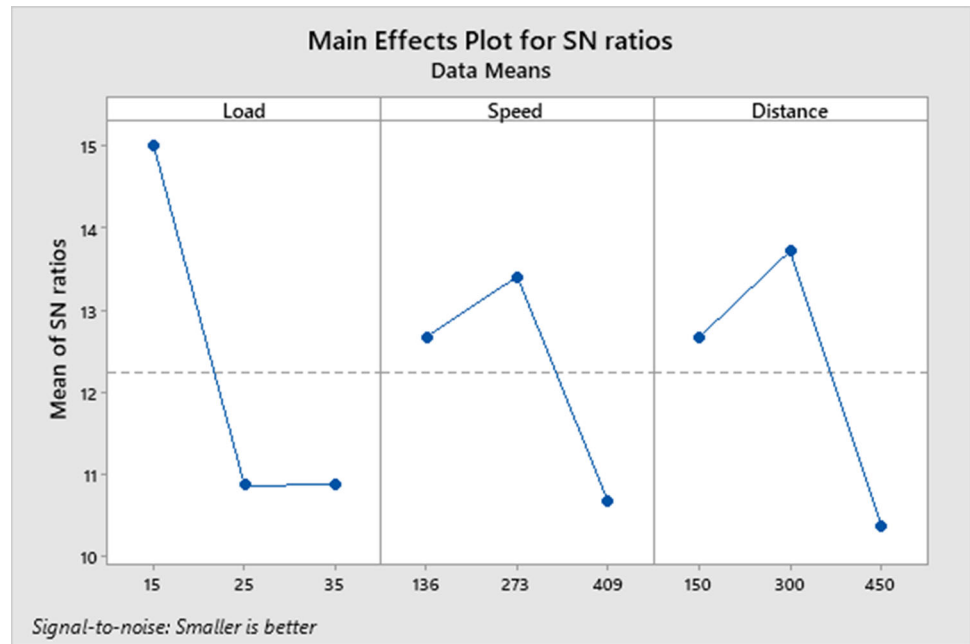


Table 5 ANOVA for WR

Source	DF	Seq SS	F-value	P-value	% of contribution
Load (N)	2	92.977	114.95	0.009	49.01
Speed (rpm)	2	26.787	33.12	0.029	14.12
Distance (m)	2	69.124	85.46	0.012	36.44
Error	2	0.809			0.43
Total	8	189.697			100

Table 6 ANOVA for COF

Source	DF	Seq SS	F-value	P-value	% of Contribution
Load (N)	2	34.583	4	0.200	47.41
Speed (rpm)	2	12.078	1.4	0.417	16.56
Distance (m)	2	17.653	2.04	0.329	24.19
Error	2	8.637			11.84
Total	8	72.951			100

tively. The residual plot was used to assess the significance of the coefficients in the projected model; if it is straight, the errors are usually distributed. Figure 9(a) and Fig. 9(b) show the residual properties and noticed that the residual shown around the straight line, which gives the developed model was appreciable [7].

Regression Equation:

$$WR = 24.1 + 6.87 \text{ Load} + 0.214 \text{ Speed} - 0.277 \text{ Distance} \quad (R^2 = 91.49\%) \quad (3)$$

$$\text{COF} = 0.029 + 0.00467 \text{ Load} + 0.000183 \text{ Speed} + 0.0002 \text{ Distance} \quad (R^2 = 56.04\%) \quad (4)$$

3.5 Wear analysis

Figure 10 illustrates the worn surface of the generated AZ31-SiC-Gr hybrid nanocomposite specimen examined at various magnification settings. The illustration clearly showed grooves, delamination, pits, micro-cracks, ridges, and abrasive wear mechanisms [32] on the worn surfaces. Ridges were created as a result of the roughness of the counter disc. Pits are created as a result of the loss of reinforcing particles. The micro crack is seen on the surface in a few places because of the low stress (15 N). However, the mechanically mixed layer (MML) was formed, which lowers the WR and COF, resulting from material transfer between

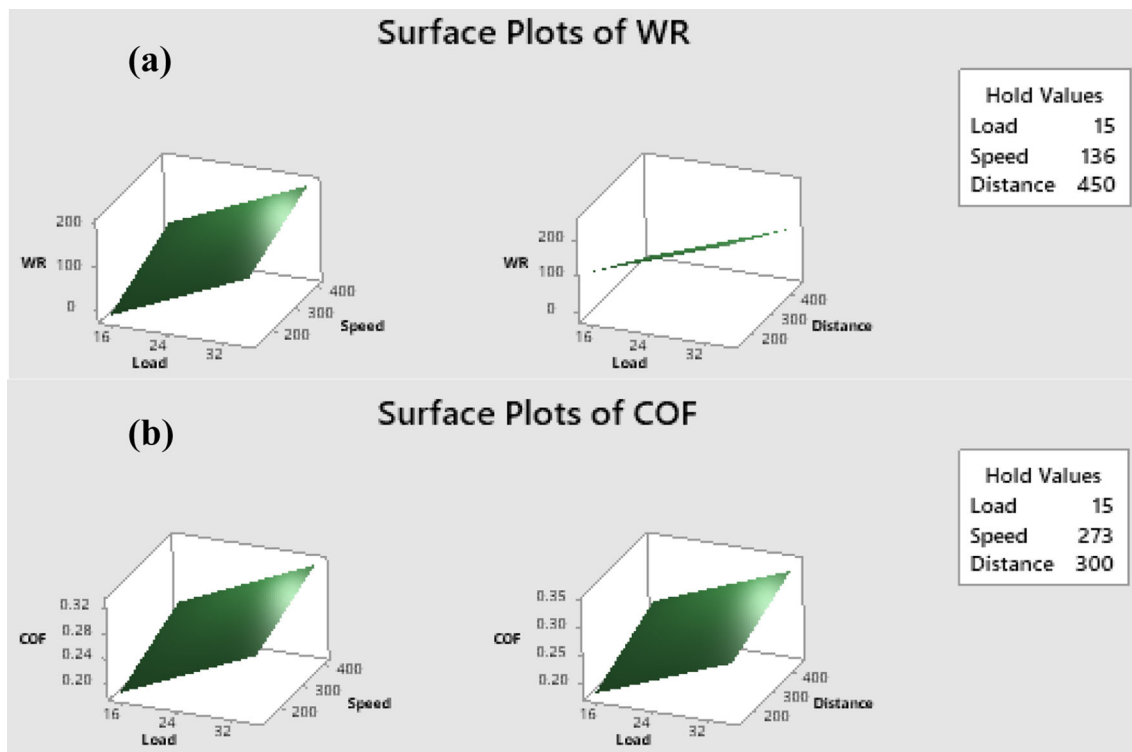


Fig. 7 a 3D Surface plot of wear rate, b 3D Surface plot of COF

the counterpart and pin surface [18, 35]. AZ31 alloys are strongly predisposed toward oxidation, which significantly impacts wear rates. Oxidative wear manifests when surfaces in contact, heated through friction, undergo oxidation. Fragile magnesium oxides break into fragments during repeated sliding movements, creating a protective oxygen layer on the surface. Direct metal-to-metal contact between the sliding surfaces is effectively avoided by this layer. The rate of wear decreases as the oxide layer on the surface thickens over time. As shown in Fig. 4, the oxygen concentration on worn surfaces was measured using EDS. The thickness of the oxide layer plays a pivotal role in influencing wear mechanisms, with this particular form of wear being termed "oxidation wear," typically categorized as mild wear. The reduction in wear rates is attributed to this unique mechanism. It has been proposed that a threshold velocity must be reached to initiate the formation of a protective oxidation film. This protective film's structural support comes from the underlying specimen. Oxidation wear tends to be most prominent within a limited range of applied load and sliding speed, as under more severe conditions, the protective oxidation layer ceases to exist.

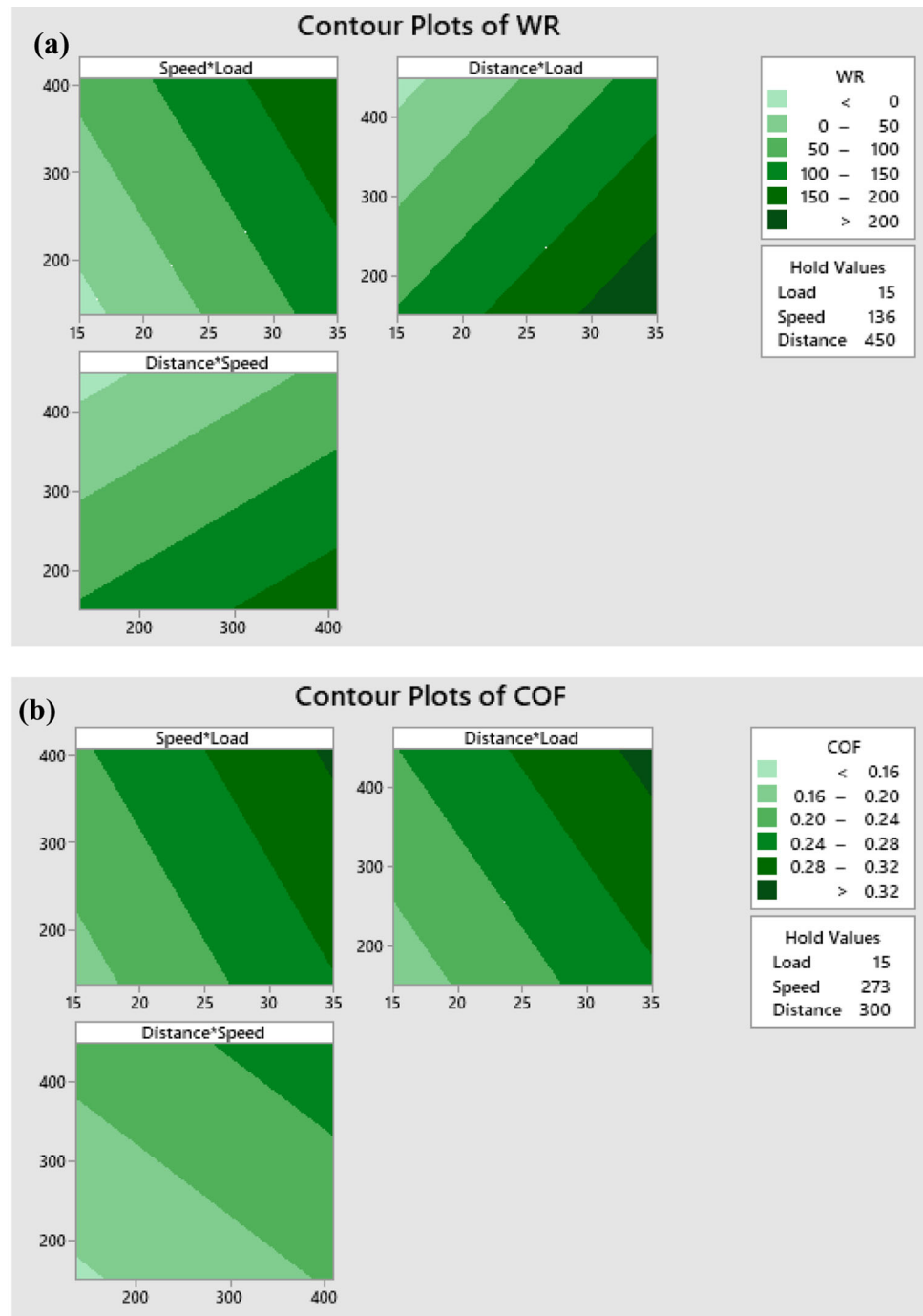
SEM micrographs illustrating the worn surface under elevated conditions of an average load (35 N) and maximum sliding distance (450 m) are presented in Figs. 10. These images depict a reduced WR for the composites subjected to the increased load. Figure 10 shows surface fractures caused

by the dissociation of nanoparticle clusters on the worn surface of the untreated composite pin. Increased sliding speed and average load cause plastic deformation on the pin's surface, which forms a layer that is work-hardened and reduces wear loss [36]. Evidence of delamination wear under these extreme conditions can be seen in the surface cracks and patches. The development and spread of cracks cause the surface to delaminate, resulting in thin sheets or flake-like formations that reduce wear resistance. Severe surface oxidation is indicated by an increase in oxide particle presence. The oxide particles in the grooves increase lubrication and wear resistance, which lowers the composites' coefficient of friction (COF) [37, 41].

The fluctuation of average COF values to sliding distance is seen in Fig. 11. These numbers show a recurrent pattern in which COF decreases as average load and sliding speed rise. All sliding situations result in a significant COF for the untreated composite. The primary cause of this large COF is the sliding-induced separation of aggregated nanoparticles from the pin surface. This third-body abrasion results in the detachable nanoparticles becoming trapped between the sliding surfaces and further abrading the pin surface, raising the COF [39].

The COF rises at slower rotating speeds as a result of the enormous exposure of the pin surface to the counterface brought on by the applied average load [40]. On the other side, as the sliding speed increases, COF values decrease. This

Fig. 8 a Contour plot of wear rate, b Contour plot of COF



drop can be due to the pin's and counterface's shorter contact times as sliding speed increases, which in turn reduces COF. Frictional heating with higher average loads and faster sliding rates is responsible for the increase in COF. It is possible to link the decrease in COF with increasing average load and sliding speed to the formation of an oxide layer, which improves lubrication [40, 46, 47]. Additionally, frictional heating causes bulk softening and plastic flow, which serve to smoothen the pin surface and lessen adhesion between the

pin and counterface surfaces [10, 39]. The wear rates of the composites as a function of sliding distance under various loads are shown in Fig. 12. The wear rate rises as the sliding distance rises, which is one obvious tendency. With increased normal loads, the composites' wear rate increases. Even if the volume of SiC and graphite nanoparticles is the same throughout all composites, it is important to note. Under all sliding situations, the untreated composite continually displays low wear resistance.

Fig. 9 a Residual plots for WR,
b Residual plots for COF

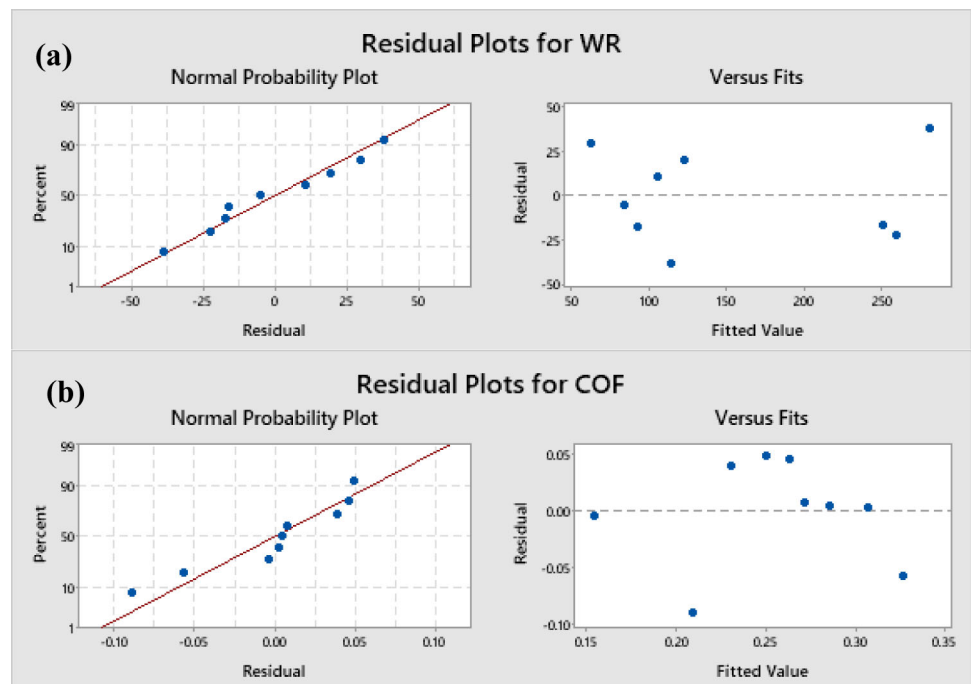
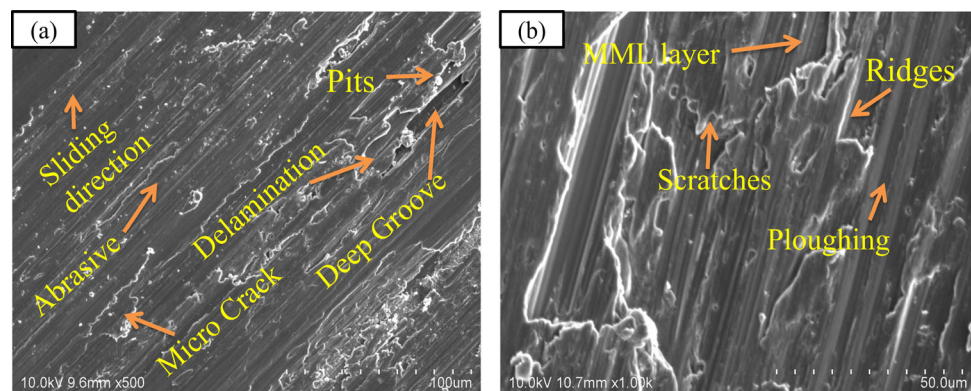


Fig. 10 SEM micrographs of nanocomposite at different magnification



4 Conclusions

- Taguchi method determined that the optimum combination for obtaining low WR was found as load 15 N, speed rpm, and distance 450 m (L1-S1-D3), and for low COF, it was seen as load 15 N, speed 273 rpm, and distance 300 rpm (L1-S2-D2) because the addition of Gr particles boosted bonding strength and reduced material dislodging.
- The ANOVA results show that load, followed by distance and speed, is the most critical determinant of wear loss—the wear rate increases as the sliding distance increases. The wear rate of the composites exhibits an increase with higher normal loads. The maximum wear rate (320 µm) was observed at a load of 35N, speed of 409 rpm with a sliding distance of 300 m, while the minimum wear rate (79 µm) was found at a load of 15N, speed of 136 rpm with a sliding distance of 150 m.
- The linear regression equation was developed for WR and COF and checked with the R² value. Hence, the developed model fits WR well, as the acceptance level is 95%.
- After the wear test, SEM analysis of the worn surface showed that micro-cracks and abrasive wear mechanisms were observed in the hybrid nanocomposite. The solid lubricant graphite in the hybrid nanocomposite increased wear resistance by establishing a lubricant layer over the sliding counterparts.
- At lower rotational speeds, the COF increases due to the enormous exposure of the pin surface to the counterface under the influence of the applied average load. The COF values decline as the sliding speed escalates. This reduction can be attributed to the decreased contact time between the pin and counterface as sliding speed advances, ultimately leading to diminished COF.

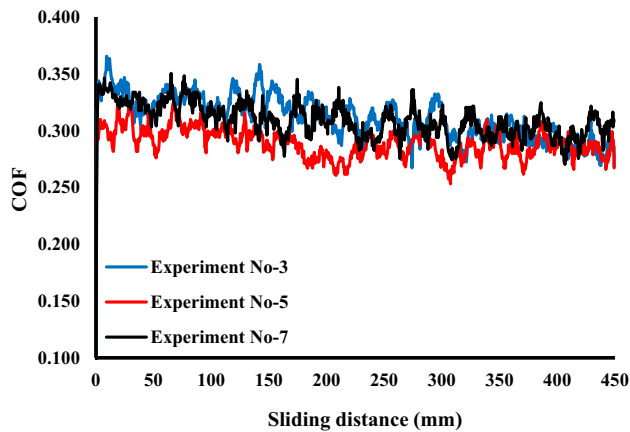


Fig. 11 Variation of COF to the sliding distance

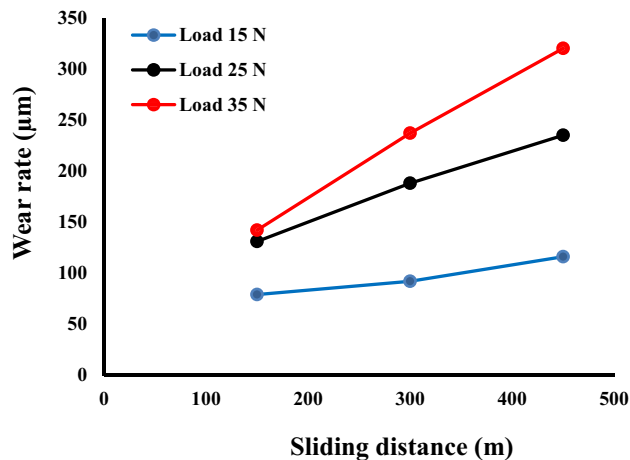


Fig. 12 Variation of wear rate to the sliding distance at different load conditions

Acknowledgements The authors wish to acknowledge the Department of Mechanical Engineering at Aditya Engineering College, India, for their valuable technical support during the execution of this experimental work. Furthermore, the authors would like to convey their appreciation to Rathinam Technical Campus for their assistance in the research of this manuscript.

Data availability The conclusions drawn from this research study are supported by the data, which has already been included in the article. Should there be a requirement for extra data or supplementary details, interested parties can contact the corresponding author to obtain them.

Declarations

Conflict of interest The authors affirm the absence of any conflicts of interest concerning the publication of this paper.

References

- Islam S.S.U., Khan N.Z., Khan M.M. Effect of reinforcement on magnesium-based composites fabricated through stir casting: A review. *Materials Today Proceedings*. 2020; 6513–6518.
- Dash D., Samanta S., Rai R.N. Study on Fabrication of Magnesium based Metal Matrix Composites and its improvement in Mechanical and Tribological Properties- A Review. *Materials Science and Engineering*. 2018.
- Nie, K.B., Wang, X.J., Deng, K.K., Hu, X.S., Wu, K.: Magnesium matrix composite reinforced by nanoparticles – A review. *Journal of Magnesium and Alloy*. **9**, 57–77 (2021)
- Seikh, Z., Sekh, M., Kunar, S., Kibria, G., Haque, R., Haidar, S.: Rice Husk Ash Reinforced Aluminium Metal Matrix Composites: A Review. *Mater. Sci. Forum* **1070**, 55–70 (2022)
- Gugulothu, B., Saminathan, R., Pradeep, A., Sharma, A., Vijayakumar, S., Paramasivam, P., & Srinivasa Rao, N. (2023). Investigating the strength of butt-welded joints of AA6082 and AA5052 alloys through friction stir welding; the impact of tool tilt angle and feed rate. *Journal of Adhesion Science and Technology*, 1–24. doi:<https://doi.org/10.1080/01694243.2023.2253631>
- Vijayakumar, S., Anitha, S., Arivazhagan, R., Hailu, A.D., Rao, T.V.J., Pydi, H.P.: Wear investigation of aluminum alloy surface layers fabricated through friction stir welding method. *Adv. Mater. Sci. Eng.* **2022**, 1–8 (2022)
- Gugulothu, B., Anusha, P., Swapna Sri, M.N., Vijayakumar, S., Periyasamy, R., Seetharaman, S.: Optimization of stir-squeeze casting parameters to analyze the mechanical properties of Al7475/B4C/Al2O3/TiB2 hybrid composites by the Taguchi method. *Adv. Mater. Sci. Eng.* **2022**, 1–9 (2022)
- Vijayakumar, S., Manickam, S., Seetharaman, S., Rao, T.V.J., Pounraj, D., Pydi, H.P.: Examination of friction stir-welded AA 6262/5456 joints through the optimization technique. *Adv. Mater. Sci. Eng.* **2022**, 1–11 (2022)
- Anusha, P., Sri, M. N. S., Vijayakumar, S., Rao, T. V. J., Paramasivam, P., Jeyakrishnan, S., & Saxena, K. K. (2023). Design and optimization the wear characteristics for Al7178/TiO2/B4C/FA central hybrid composite. *International Journal on Interactive Design and Manufacturing (IJDeM)*.
- Vijayakumar, S., Arunkumar, A., Pradeep, A., Satishkumar, P., Singh, B., Rama Raju, K. S., & Sharma, V. K. (2023). Optimization of process variables for shielded metal arc welding dissimilar mild steel and medium carbon steel joints. *Journal of Adhesion Science and Technology*, 1–18.
- Sharma, P., Paramasivam, P., Bora, B.J., Sivasundar, V.: Application of nanomaterials for emission reduction from diesel engines powered with waste cooking oil biodiesel. *International Journal of Low-Carbon Technologies* **18**, 795–801 (2023). <https://doi.org/10.1093/ijlct/ctad060>
- Alizadeh, A., Khayami, A., Karamouz, M., Hajizamani, M.: Mechanical properties and wear behavior of Al5083 matrix composites reinforced with high amounts of SiC particles fabricated by combined stir casting and squeeze casting: A comparative study. *Ceram. Int.* **48**, 179–189 (2022)
- Anusha, P., Sri, M.N.S., Vijayakumar, S., Rao, T.V.J., Paramasivam, P., Jeyakrishnan, S., Saxena, K.K.: Design and optimization the wear characteristics for Al7178/TiO2/B4C/FA central hybrid composite. *Int. J. Interact. Des. Manuf. (IJDeM)* (2023). <https://doi.org/10.1007/s12008-023-01341-5>

14. Paramasivam, P., Vijayakumar, S.: Mechanical characterization of aluminium alloy 6063 using destructive and non-destructive testing. *Mater. Today Proc.* **81**, 965–968 (2021)
15. Gugulothu, B., Karumuri, S., Vijayakumar, S., Muthuvel, B., Seetharaman, S., Jeyakrishnan, S., Saxena, K.K.: Optimization of TIG welding process parameters on chrome alloy steel using box-behnken method. *Int. J. Interact. Des. Manuf. (IJIDeM)* **5**, 1–13 (2023). <https://doi.org/10.1007/s12008-023-01531-1>
16. Srinivasan, D., Meignanamoorthy, M., Gacem, A., Vinayagam, M., Sathish, T., Ravichandran, M., Srinivasan, S.K., Abdellatif, M.H., Allasi, H.L.: Tribological behavior of Al/nanomagnesium/aluminum nitride composite synthesized through liquid metallurgy technique. *J. Nanomater.* **24**, 1–12 (2022)
17. Swamy, A., Shamitha, C., Singh, M.K., Rinawa, M.L., Kumar, K.V.P., Obaid, S.A., Mahadik, M.A., Alfarraj, S., Markos, M.: Experimental investigations on the wear behaviour of eutectic Al-7075/CNT/graphite composites manufactured by a combination of two-stage stir and squeeze casting techniques. *J. Nanomater.* **8**, 202 (2022)
18. Balaji, S., Maniarasan, P., Alagarsamy, S.V., Alswieleh, A.M., Mohanavel, V., Ravichandran, M., Jeon, B.H., Allasi, H.L.: Optimization and prediction of tribological behaviour of Al-Fe-Si alloy-based nanograin-refined composites using taguchi with response surface methodology. *J. Nanomater.* **2022**, 1–12 (2022)
19. Subramani, M., Huang, S.J., Borodianskiy, K.: Effect of SiC nanoparticles on AZ31 magnesium alloy. *Materials* **15**, 1004 (2022)
20. Khatkar, S.K., Verma, R., Kharb, S.S., Thakur, A., Sharma, R.: Optimization and effect of reinforcements on the sliding wear behavior of self-lubricating AZ91D-SiC-Gr hybrid composites. *SILICON* **13**, 1461–1473 (2021)
21. Gnanavelbabu, A., Sunu Surendran, K.T., Kumar, S.: Influence of ultrasonication power on grain refinement, mechanical properties and wear behaviour of AZ91D/nano-Al₂O₃ composites. *Mater. Res. Exp.* **7**, 16544 (2019)
22. Ambigai, R., Prabhu, S.: Optimization of friction and wear behaviour of Al–Si₃N₄ nano composite and Al–Gr–Si₃N₄ hybrid composite under dry sliding conditions. *Trans. Nonferr. Metals Soc.* **27**, 986–997 (2017)
23. Kaushik, N.C., Rao, R.N.: The effect of wear parameters and heat treatment on two body abrasive wear of Al-SiC-Gr hybrid composites. *Tribol. Int.* **96**, 184–190 (2016)
24. Suresh, S., Gowd, G.H., Deva Kumar, M.L.S.: Wear behaviour of Al 7075/SiC/Mg metal matrix nano composite by liquid state process. *Adv. Compos. Hybrid Mater.* **1**, 819–825 (2018)
25. Xiao, P., Gao, Y., Xu, F., Yang, C., Li, Y., Liu, Z., Zheng, Q.: Tribological behavior of in-situ nanosized TiB₂ particles reinforced AZ91 matrix composite. *Tribol. Int.* **128**, 130–139 (2018)
26. Arunachalam, U., Vairamuthu, J.: Tribological analysis on magnesium alloy AZ31B with reinforced ZrSiO₄ through Taguchitechnique. *Mater. Today Proc.* **37**, 2521–2528 (2021)
27. Kannan, G., Thangaraju, R., Cabrera, F.M.: Sustainable development of agro-industrial waste-based banana fiber/fly ash polyester composites for wear and friction study. *J. Natl. Fibers* **16**, 14771 (2022)
28. Mohammed, A.A., Khan, A.S.A., Baig, M.: Optimization of dry sliding wear behavior of aluminium-based hybrid MMC's using experimental and DOE methods. *J. Market. Res.* **16**, 743–763 (2022)
29. Kumar, A., Rana, R.S., Purohit, R., Namdev, A., Saxena, K.K., kumar, A.: Optimization of dry sliding wear behavior of Si₃N₄ and Gr reinforced Al–Zn–Mg–Cu composites using taguchi method. *J. Mater. Res. Technol.* **19**, 4793–4803 (2022)
30. Kumar, B.S.P., Shobha, K.R., Singh, M.K., Rinawa, M.L., Madhavarao, S., Wadhawa, G.C., Alrebdi, T.A., & Christopher, D.: Optimization and wear properties for the composites of metal matrix AA8011/boron nitride using Taguchi method. In P. Velmurugan (Ed.), *Journal of Nanomaterials* (Vol. 2022, pp. 1–10).
31. Khan, M.M., Dey, A., Hajam, M.I.: Experimental investigation and optimization of dry sliding wear test parameters of aluminum based composites. *SILICON* **14**, 4009–4026 (2022)
32. Akbari, M., Asadi, P.: Optimization of microstructural and mechanical properties of brass wire produced by friction stir extrusion using Taguchi method. *J. Mater. Des. Appl.* **27**, 2709 (2021)
33. Asadi, P., Akbari, M., Givi, M.K.B., Panahi, M.S.: Optimization of AZ91 friction stir welding parameters using Taguchi method. *J. Mater. Des. Appl.* **230**(1), 291–302 (2015)
34. Veeranjeyulu, I., Chittaranjan Das, V., & Karumuri, S.: Investigation of mechanical properties and microstructure of AZ31-SiC-graphite hybrid nanocomposites fabricated by bottom pouring-type stir casting machines. In T. Varol (Ed), *Advances in Materials Science and Engineering* (Vol. 2023, pp. 1–8) (2023)
35. Saravanakumar, R., Rajasekaran, T., Pandey, C. Optimisation of underwater friction stir welding parameters of aluminum alloy AA5083 using RSM and GRA. In *Proceedings of the Institution of Mechanical Engineers, Part E: Journal of Process Mechanical Engineering* (p. 095440892211344).
36. Banerjee, S., Poria, S., Sutradhar, G., Sahoo, P.: Dry sliding tribological behavior of AZ31-WC nanocomposites. *J. Magnes. Alloys.* **7**, 327315 (2019)
37. Sirajudeen, N., Abdur Rahman, M., Serajul, H., Karunanithi, R., Subhrajit, P.: Influence of aging & varying weight fraction of Al₂O₃ particles on the mechanical behaviour & volumetric wear rate of Al 7075 alloy composite produced by liquid metallurgy route. *Mater. Res. Express* **6**, 086597 (2019)
38. Rana, H., Badheka, V., Kumar, A., Satyaprasad, A.: Strategical parametric investigation on manufacturing of Al–Mg–Zn–Cu alloy surface composites using FSP. *Manuf. Processes* **33**, 545534 (2017)
39. Mehdi, H., Mishra, R.S.: Effect of friction stir processing on mechanical properties and wear resistance of tungsten inert gas welded joint of dissimilar aluminum alloys. *J. Mater. Eng. Perform.* **30**, 1926–1937 (2021)
40. Hashmi, A.W., Mehdi, H., Mabuwa, S., VelaphiMsomi, P.M.: Influence of FSP parameters on wear and microstructural characterization of dissimilar TIG welded joints with Si-rich filler metal. *Silicon* **14**, 11131–11145 (2022)
41. Prakash Pasupulla, A., Abebe Agisho, H., Seetharaman, S., Vijayakumar, S.: Characterization and analysis of TIG welded stainless steel 304 alloy plates using radiography and destructive testing techniques. *Mater. Today Proc.* **51**, 935–938 (2022). <https://doi.org/10.1016/j.matpr.2021.06.305>
42. Pal, D., Vijayakumar, S., Rao, T.V.J., Babu, R.S.R.: “An examination of the tensile strength, hardness and SEM analysis of Al 5456 alloy by addition of different percentage of SiC/flyash. *Mater. Today Proc.* **62**, 1995 (2022). <https://doi.org/10.1016/j.matpr.2022.02.288>

43. Karumuri, S., Haldar, B., Pradeep, A., Karanam, S.A.K., Sri, M.N.S., Anusha, P., Vijayakumar, S.: Multi-objective optimization using Taguchi based grey relational analysis in friction stir welding for dissimilar aluminium alloy. *Int. J. Interact. Des. Manuf. (IJIDeM)*. (2023). <https://doi.org/10.1007/s12008-023-01529-9>
44. Pydi, H.P., Pasupulla, A.P., Vijayakumar, S., Agisho, H.A.: Study on microstructure, behavior and Al₂O₃ content flux A-TIG weldment of SS-316L steel. *Mater. Today Proc.* **51**, 728–734 (2022). <https://doi.org/10.1016/j.matpr.2021.06.218>
45. Vijayakumar, S., Dhasarathan, N., Devabalan, P., Jehan, C.: Advancement and design of robotic manipulator control structures on cyber physical production system. *J. Comput. Theor. Nanosci.* **16**(2), 659–663 (2019). <https://doi.org/10.1166/jctn.2019.7786>
46. Pradeep, A., Kavitha, N., Janardhana Rao, T.V., Vijayakumar, S.: Influence of nano alumina/vegetable oil based cutting fluid on MQL turning of stainless steel 304. *Mater. Today Proc.* (2022). <https://doi.org/10.1016/j.matpr.2022.06.547>
47. Boopathy, G., Vanitha, V., Karthiga, K., Gugulothu, B., Pradeep, A., Pydi, H.P., Vijayakumar, S.: Optimization of tensile and impact strength for injection moulded nylon 66/SiC/B4c composites. *J. Nanomater.* **2022**, 1–9 (2022). <https://doi.org/10.1155/2022/4920774>

Publisher's Note Springer Nature remains neutral with regard to jurisdictional claims in published maps and institutional affiliations.

Springer Nature or its licensor (e.g. a society or other partner) holds exclusive rights to this article under a publishing agreement with the author(s) or other rightsholder(s); author self-archiving of the accepted manuscript version of this article is solely governed by the terms of such publishing agreement and applicable law.